

DISCUSSION PAPERS OF ISDS
99-24, DUKE UNIVERSITY

Estimating Global and Local Scaling Exponents in Turbulent Flows using Wavelet Transformations

BY

GABRIEL KATUL

School of Environment, Duke University, Durham, NC 27708-0328

BRANI VIDAKOVIC

*Institute of Statistics and Decision Sciences, Duke University, Durham, NC
27708-0251*

AND

JOHN ALBERTSON

*Department of Environmental Sciences, University of Virginia, Charlottesville, VA
22903*

July 19, 1999.

Abstract. High frequency longitudinal velocity (u) measurements were performed in the atmospheric boundary layer to investigate the inertial subrange structure of turbulence. Global and local scaling exponent distributions and other statistical properties were derived using continuous (CWT) and critically sampled orthonormal (OWT) wavelet transformations. These statistical measures were contrasted to similar statistical measures derived by applying CWT and OWT to a fractional Brownian motion (fBm) time series with a Hurst exponent of $1/3$. This study demonstrated that both CWT and OWT were able to resolve intermittency-based departures from global power-laws observed in higher-order structure functions. Particularly, the global power laws inferred from OWT were in excellent agreement with the She-Lévêque vortex filament model. However, these wavelet computed intermittency departures were smaller than those computed by the extended self similarity structure function approach. The effects of vortex stretching on the dimensionless structure skewness were well captured by CWT and OWT coefficients. However, the CWT was not able to discern any fundamental differences in the u and fBm local scaling exponent distributions.

1 Introduction

Arguments that turbulence is not exactly self similar, exhibits multifractal behavior, and possesses a distribution of local scaling exponents, were based on global statistical properties such as higher-order structure functions^{1,2}. Because of its fundamental basis³⁻⁶, much research effort was dedicated to using continuous wavelet transformations (*CWT*) to estimate these local scaling exponents².

In particular, Bacry *et al.*⁷ were the first to report distributions of local scaling exponents calculated via *CWT*. Their results suggest that *CWT* can be used to estimate local scaling exponents characterizing the multifractal behavior of velocity fluctuations without resorting to measures of turbulent kinetic energy dissipation. Additionally, their wind-tunnel measurements demonstrated that the most probable local scaling exponent is that derived from the Kolmogorov⁸ scaling [hereafter referred to as **K41**] with a distribution which supports the multifractal model of Parisi-Frisch⁹. The main conclusions in Bacry *et al.*⁷ and others^{10,11} demonstrate the potential usefulness of *CWT* in understanding the local structure of turbulence.

The important role of local scaling exponents in developing a coherent theoretical framework for inertial subrange turbulence¹²⁻¹⁴ motivated us to further explore their estimation via *CWT*. Particularly, our objective is to rigorously evaluate whether *CWT* can delineate significant differences in local scaling exponents in turbulence measurements when contrasted with fractional Brownian motion (*fBm*) time series exhibiting identical **K41** global scaling laws, but being devoid of the vortex stretching signature and multi-fractality. In fact, other researchers who utilized critically sampled orthogonal wavelet transformations (*OWT*) argued that the redundancy in *CWT* may well distort wavelet coefficients to the extent that dynamic properties of inertial subrange turbulence are masked rather than revealed¹⁵⁻¹⁸. To date, detailed comparisons between power-laws inferred from *OWT* and *CWT* coefficients derived from the same data set has not been performed. Such a comparison is presented here.

2 Theory

In this section **K41** theory, properties of *fBm*, and the selection of the analyzing wavelet are reviewed. The appendix provides an overview of *CWT* and *OWT*.

2.1 K41 Scaling

A property of the turbulent velocity differences ($u(x+r) - u(x)$) between two points separated by a distance r within the inertial subrange, for order $n > 1$, is given by

$$\langle [u(x+r) - u(x)]^n \rangle = C_n \langle \epsilon \rangle^{\frac{n}{3}} r^{\frac{n}{3}}, \quad (1)$$

where C_n are similarity constants (except for C_3) and $\langle \cdot \rangle$ denotes averaging. The turbulent kinetic energy dissipation rate ϵ is given by

$$\epsilon = \nu \langle s_{ij} s_{ij} \rangle,$$

where ν is the fluid kinematic viscosity, $s_{ij} = \left(\frac{\partial u_i}{\partial x_j} + \frac{\partial u_j}{\partial x_i} \right)$ is the strain rate tensor, u_1 (or u) is the turbulent longitudinal velocity component, u_2 (or v) is the turbulent lateral velocity component, and u_3 (or w) is the turbulent vertical velocity component, with $\langle u_i \rangle = 0$, x_i ($x_1 = x, x_2 = y, x_3 = z$) are the longitudinal, lateral, and vertical directions, respectively.

The above **K41** scaling laws hold for $\eta < r < L_u$, where $\eta = (\nu^3 / \langle \epsilon \rangle)^{1/4}$ is the Kolmogorov dissipation length scale and L_u is the integral length scale defined as

$$L_u = \frac{1}{\sigma_u^2} \int_0^\infty \langle u(x)u(x+r) \rangle dr,$$

for a stationary u .

2.2 Overview of Fractional Brownian Motion Statistical Properties

Energy cascades generated from solutions of the Navier-Stokes equations are often contrasted with cascades generated by strictly self similar processes, such as fractional Brownian motion (*fBm*) to highlight multifractal properties of turbulence¹¹.

The *fBm* is a Gaussian, zero mean, continuous, non-stationary process, indexed by the parameter H (Hurst exponent, $0 < H < 1$) such that

$$B_H(0) = 0, \text{ and} \\ B_H(t+r) - B_H(t) \sim \mathcal{N}(0, \sigma_H^2 |r|^{2H}),$$

where

$$\sigma_H^2 = \Gamma(1-2H) \frac{\cos \pi H}{\pi H},$$

and $\Gamma(x) = \int_0^\infty t^{x-1} e^{-t} dt$ is the Gamma function¹⁹⁻²².

From its definition, the sample paths of *fBm* satisfy the scaling equation $B_H(at) \stackrel{d}{=} a^H B_H(t)$, and

$$\langle |B_H(t+r) - B_H(t)|^n \rangle = C_{fBm} \cdot |r|^{nH}, \quad (2)$$

where the C_{fBm} is

$$\sigma_H^2 \frac{2^{n/2}, \left(\frac{n+1}{2}\right)}{\left(\frac{1}{2}\right)},$$

and where $\stackrel{d}{=}$ is *equal in distribution*.

The Fourier transformation of (2) is proportional to $\frac{1}{|\omega|^{n(H+1/2)}}$ with an average power spectrum proportional to $\frac{1}{|\omega|^{2H+1}}$. For $H = \frac{1}{3}$ all **K41** global power laws are theoretically satisfied for any n .

2.3 Selection of Wavelets

In wavelet transformations, the choice of the analyzing wavelet remains subjective. Due to its wide usage in turbulence research²³, and its suitability to this problem, we selected the “Haar” wavelet whose definition and properties are given in the appendix. The Haar wavelet satisfies the admissibility condition²⁴ described in the appendix for *CWT*. The Haar wavelet is antisymmetric so that statistical measures sensitive to vortex stretching can be well captured via its wavelet coefficients.

3 Experiment

Time series measurements were collected over the Duke Forest near Durham, North Carolina. In this data set, $21Hz$ velocity, and virtual potential temperature were collected on June, 18 1996, 8:00 am EST, at 40 *m* above the ground surface, in a 33 *m* tall forest, using a GILL triaxial sonic anemometer. The measurements were subsequently divided into 26 minute intervals to produce $N = 32,768$ time measurement per run. Here we focus on one such run, typical of the ensemble of runs collected in this experiment^{25,26}. For this run, the turbulent intensity was less than 0.1, and atmospheric stability was nearly neutral. In order to perform comparisons with a simulated *fBm* time series, the sample velocity run was normalized to zero-mean and unit variance.

4 Results

In this section, we first identify the delimiters of the inertial subrange via higher order ($n > 2$) structure functions. Next, we determine whether both *CWT* and *OWT* can reproduce the global scaling exponents for u and *fBm*. A critical assessment of the ability of *CWT* to distinguish between the u and *fBm* local scaling exponents is then presented.

4.1 Identification of Inertial subrange from Measured Structure Functions

To identify the inertial subrange, the second ($n = 2$) and third ($n = 3$) order structure functions are first computed. The time increments were then converted to spatial

increments using Taylor’s hypothesis²⁷. The separation distance (i.e. eddy size) range for which simultaneous $r^{2/3}$ and r^{-1} power laws exist was noted and used in the \mathcal{CWT} analysis.

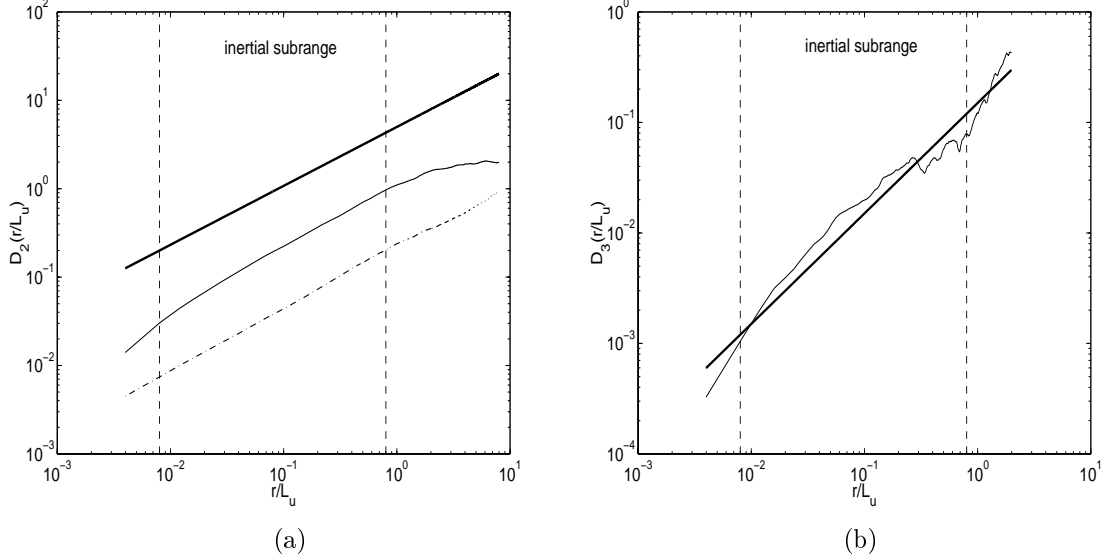


Figure 1: Identification of inertial subrange using $D_2(r)$ and $D_3(r)$. The separation distance r is normalized by the integral scale L_u . In panel (a), the solid line is for u and the dashed is for fBm . The solid-thick lines represent **K41** power-laws. For fBm , the $D_3(r) \approx 0$ and is not shown.

Figure 1 (a) shows the computed $D_2(r)$ for the u and fBm . For a more stringent criteria for onset of the inertial subrange, $D_3(r)$ is also used^{28–31}. In both panels, the inertial subrange delimiters are shown. Here, the apparent dissipation at the finest scales is due to averaging fluctuations across the sonic path length ($= 15\text{ cm}$). About two decades of inertial subrange exist for this run. The $D_3(r)$ scaling will form the basis of our assessment of \mathcal{CWT} and \mathcal{OWT} . Our choice of $D_3(r)$ stems from the fact that $D_3(r)$ is the only structure function whose scaling form can be predicted analytically from the Navier-Stokes equations² for locally homogeneous and isotropic turbulence. It is given by

$$\langle [u(x+r) - u(x)]^3 \rangle = -\frac{4}{5} \langle \epsilon \rangle r$$

while for an fBm process,

$$\langle [u(x+r) - u(x)]^3 \rangle = 0$$

Hence, in this context, fBm processes are in stark contrast to high Reynolds number turbulent flows for which $D_3(r)$ must be non-vanishing to permit vortex stretching

(irrespective of the validity of **K41** or other local isotropy approximations). Additionally attractive is that $D_3(r)$ is linearly related to $\langle \epsilon \rangle$ and does not suffer from intermittency corrections.

4.2 Determination of Global Exponents

The global scaling exponents can be readily determined from the coefficients of \mathcal{CWT} or \mathcal{OWT} using

$$\langle |\mathcal{CWT}_u(a, \cdot)|^n \rangle = C_\beta a^\beta,$$

where β is the global exponent (which must be identical to $-5n/6$ to recover **K41** power-laws in the frequency domain), C_β are constants related to the **K41** similarity constants (C_n) and $\langle \epsilon \rangle$, and $\langle \cdot \rangle$ is averaging across location for each scale a . Unless otherwise stated, we report **K41** scaling in the frequency domain for \mathcal{CWT} and \mathcal{OWT} , and in the time domain for higher-order structure functions.

Figure 2 demonstrates that well defined global power-laws exist in \mathcal{CWT} and \mathcal{OWT} coefficients of u within the inertial subrange. Interestingly, the inertial subrange identified from $D_3(r)$ is co-located with the inertial subrange identified from \mathcal{CWT} and \mathcal{OWT} even for $n = 6$. For comparison with u , the fBm global scaling exponents determined by \mathcal{CWT} and \mathcal{OWT} are also shown for $n = 2, 3$, and 6 along with **K41** power-laws. It is evident that both \mathcal{CWT} and \mathcal{OWT} global scaling exponents match the theoretical power laws for the fBm process. For the u time series, some departure from **K41** power-laws is noted, particularly for $n = 6$. Whether such departure is an artifact of the wavelet transformation or is produced because of intermittency effects is considered next. Particularly, we consider two indirect tests to assess how well \mathcal{CWT} and \mathcal{OWT} reproduce global power-laws for u : the intermittency corrections to **K41** power-laws and the effect of vortex stretching on the dimensionless structure skewness. We also perform the same two tests on the fBm time series but using the u inertial subrange delimiters to assess distortions to **K41** power-laws due to limited sample size, exponent determination method, and other factors leading to artificial intermittency buildup with increasing n .

To assess how well \mathcal{CWT} and \mathcal{OWT} reproduce intermittency corrections, consider again the general n th order structure function given by

$$\langle |u(x+r) - u(x)|^n \rangle \propto r^{\zeta_n}, \quad (3)$$

where, $\zeta_n = \frac{n}{3}$ for **K41**, $\zeta_n = \frac{n}{3} + (3-D)(1 - \frac{n}{3})$ for the mono-fractal β model with fractal dimension D , $\zeta_n = \frac{n}{3} + \frac{\mu}{18}(3n - n^2)$, where μ is the Kolmogorov intermittency parameter for the lognormal model³², $\zeta_n = \inf_h [nh + 3 - D(h)]$ for the Parisi-Frisch multifractal model of generalized dimensions $D(h)$, to list a few². Figure 3 computes ζ_n using the structure function approach and using the global scaling exponents determined from the coefficients of \mathcal{CWT} and \mathcal{OWT} for both u and fBm . Estimating

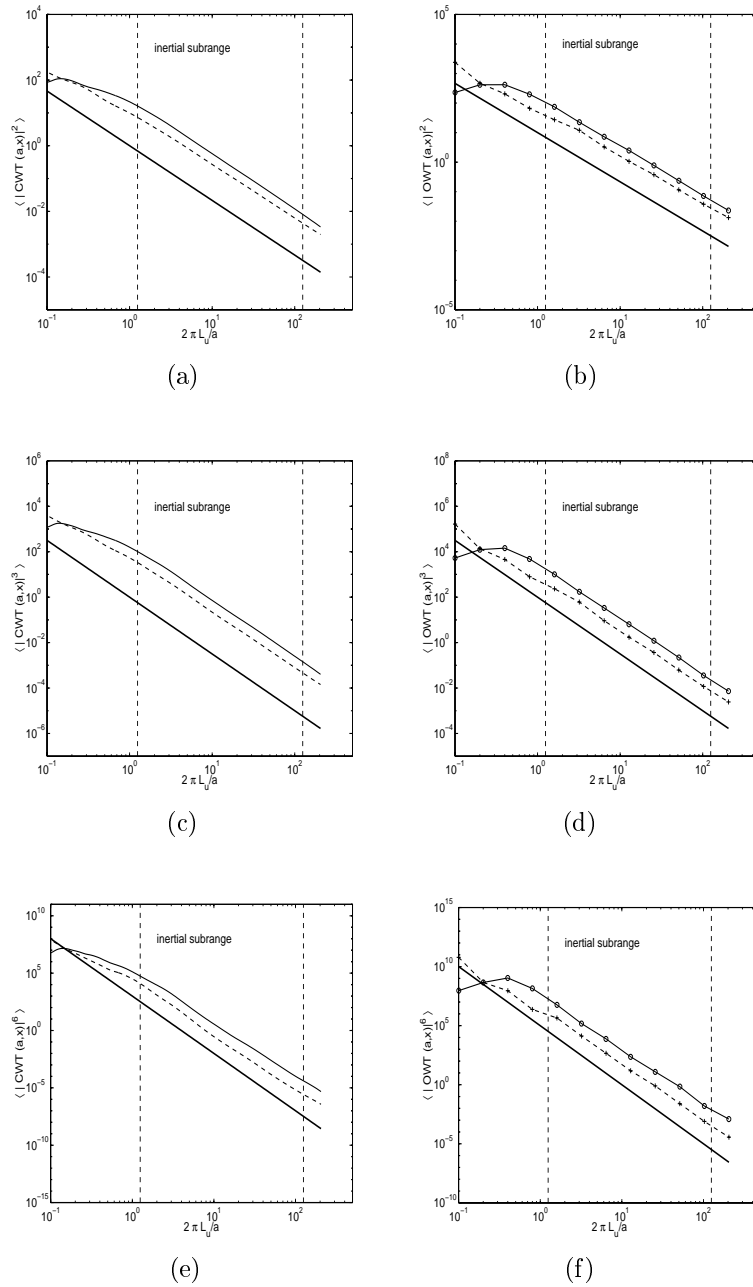


Figure 2: Determination of the global scaling exponents from CWT (left) and OWT (right) for $n = 2$, $n = 3$, and $n = 6$, with the solid and dashed lines representing the u and fBm time series. The **K41** power-laws $(-5/3, -5/2, -5)$ are also shown. The scale a is normalized by the integral scale L_u for consistency with $D_n(r)$.

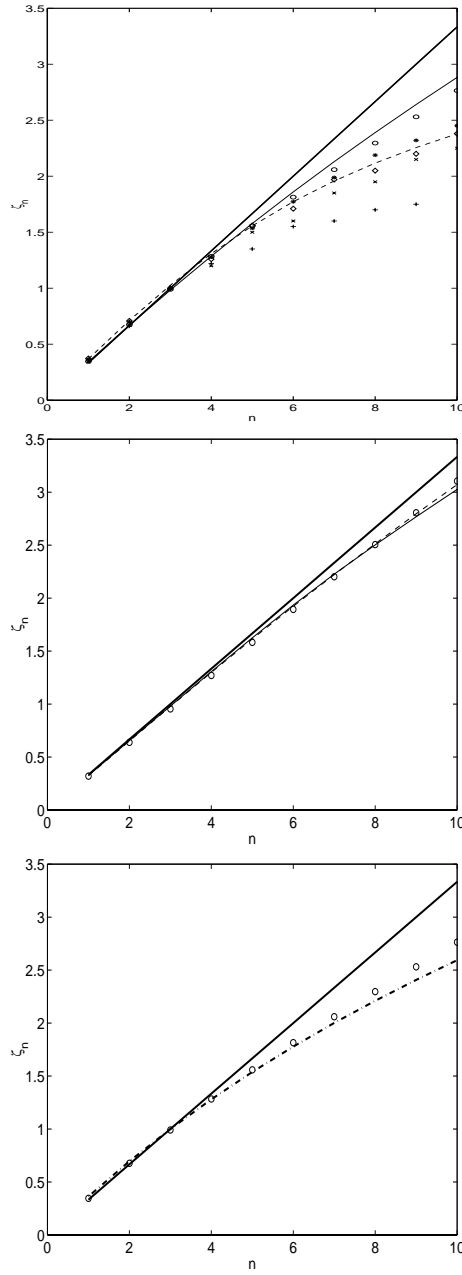


Figure 3: (a) Determination of ζ_n for $n = 1, 2, \dots, 10$ using the structure function approach (dashed-dot line), \mathcal{CWT} (solid line), and \mathcal{OWT} (\circ) for the u time series. The **K41** $\zeta_n = \frac{n}{3}$ is shown (solid-thick line). The measurements from other studies are as follows: \times are boundary layer measurements from Meneveau *et al.*³³, $+$ are boundary layer measurements from Van Atta and Chen³⁴, \star are from direct numerical simulations of isotropic turbulence from Sreenivasan and Dhruva¹³, and \diamond are from atmospheric surface layer experiments from Sreenivasan and Dhruva¹³. Measurements from Anselmet *et al.*²⁸ (not shown) closely follow Meneveau *et al.*³³. (b) Same as (a) but for the fBm . (c) Comparison between ζ_n determined from \mathcal{OWT} (\circ) coefficients and modeled by the She-Lévêque³⁵ approach (dot-dashed line). For reference, the **K41** ζ_n is also shown (solid-thick line)

ζ_n from the n th order structure function reveals the common multi-fractal behavior in u but not in the fBm .

We recognize that for large n , stability of the averaging operation may be questionable for such limited sample size². However, what is important in Figure 3 is the contrast between ζ_n for fBm and u as determined by the structure function. Even for such a limited sample size (32,768 points), the structure function approach estimated well the theoretical ζ_n for fBm up to $n = 10$. The structure function-estimated ζ_n is in excellent agreement with a wide range of measurements (see symbols in Figure 3, panel (a)) except for one data set³⁴. The latter measurements greatly suffer from limited sample size for $n > 4$. For the fBm time series, good agreement between the structure function and CWT and OWT global power-laws is noted. However, for the u time series, the structure function approach suggests greater intermittency corrections to **K41** power-laws when compared to CWT and OWT calculations, particularly if the direct numerical simulations and laboratory measurements are used as benchmarks in such a comparison. It must be emphasized that the literature reported ζ_n in Figure 3 were estimated by the so-called *extended self similarity* or *ESS* structure function method, which may underestimate ζ_n as discussed in Frisch². In fact, ζ_n estimated by OWT is in good agreement with the She-Lévêque³⁵ vortex filament intermittency model

$$\zeta_n = \frac{n}{9} + 2 - 2 \left(\frac{2}{3} \right)^{\frac{n}{3}}$$

as evidenced by Figure 3 (panel c). We reiterate here that unlike previous intermittency correction models, the She-Lévêque model has no adjustable parameters. The CWT computed intermittency correction to **K41** power-laws were consistently smaller when compared to the structure function, OWT , and the She-Lévêque³⁵ vortex filament intermittency models.

In short, CWT and OWT both capture comparable intermittency corrections to **K41** power-laws, but underestimate such **K41** corrections when compared to the *ESS* or generic structure function approaches.

To assess whether CWT and OWT capture vortex stretching effects on third-order statistics, we computed the dimensionless wavelet structure skewness (WSS) at each scale a using

$$WSS = \frac{\langle [CWT(a, \cdot)]^3 \rangle}{\langle [CWT(a, \cdot)]^2 \rangle^{3/2}}$$

The measure WSS is analogous to the third order structure function presented in Figure 2 (but without an absolute value). Using CWT and OWT , we computed the WSS for both u and fBm . Both CWT and OWT resulted in a zero WSS for fBm and a non-zero WSS for u . In fact, the OWT reproduced well the near-constant structure skewness ($= 0.25$) derived from the Kolmogorov constant [$C_3/C_2^{3/2} = (4/5)/2.2^{3/2}$].

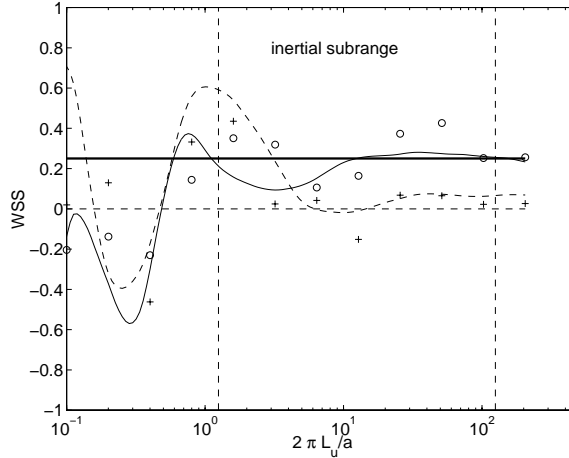


Figure 4: Wavelet structure skewness variation WSS with scale a for fBm (dashed) and u (solid) using \mathcal{CWT} . For comparison, the WSS estimated from \mathcal{OWT} are shown with $+$ for fBm and \circ for u . The inertial subrange scales are repeated for clarity (dashed vertical lines). The dashed horizontal line is $WSS=0$, and the solid line is $WSS=0.25$ determined from the Kolmogorov constant.

The constant structure skewness value from this experiment is in good agreement with other atmospheric boundary layer experiments³⁰. It must be emphasized here that an antisymmetric wavelet, such as Haar, is necessary to reproduce a non-zero WSS in the u time series. If a symmetric wavelet is used (e.g. Marr wavelet or Mexican Hat), the computed WSS will be zero as it would lack the directional differencing attribute of an antisymmetric basis function.

4.3 Determination of Local Exponents

One of the main motivations for using \mathcal{CWT} is attributed to its ability to estimate local scaling exponents⁷. The local scaling exponents can be estimated from \mathcal{CWT} using local regularity results⁶. At locations where u has a Lipschitz regularity³ α , the localized energy $(\mathcal{CWT}_u(a, b))^2$ behaves as $a^{2\alpha+1}$, for a within the inertial subrange. Hence α at position b can be estimated from the local energy spectrum³⁶. To illustrate the estimation of α , consider 50 seconds of the u time series measurements (Figure 5 a) in concert with their $(\mathcal{CWT}_u(a, b))^2$. We estimated α at $b = 10s$ (small u time gradient) and at $b = 32.4s$ (large u time gradient) using two methods (Figure 5): (i) Regressing $\log_2([\mathcal{CWT}_u(a, b)]^2)$ on $\log_2 a$, and (ii) computing the slope estimator via a Bartlett robust regression³⁷ for the range of scales in the inertial subrange. We found that the two methods provide comparable estimates of α . We applied these

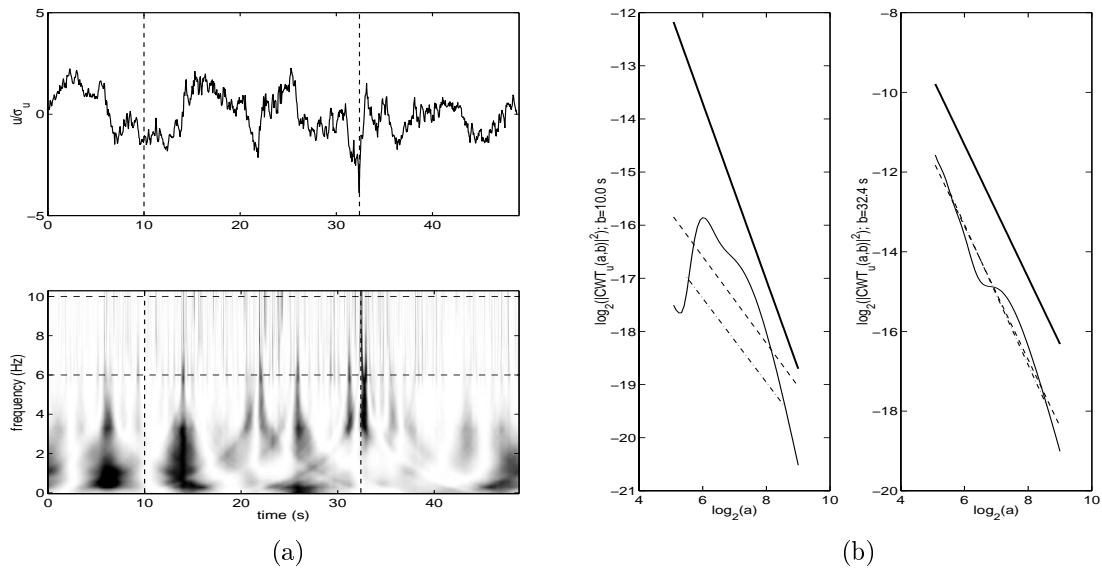


Figure 5: Panel (a) Sample u variation with time for 50 seconds duration (top) and its CWT energy distribution in the time/frequency domain. Vertical dashed lines are for $t = 10.0$ s and $t = 32.4$ s. The horizontal dashed lines delimit the inertial subrange. Panel (b) local wavelet spectra for $t = 10.0$ s and $t = 32.4$ s. The estimated local scaling exponent α for $t = 10.0$ s and $t = 32.4$ s by the regression method are -0.82 and -1.68 , respectively, and by the Bartlett method -0.79 , and -1.75 , respectively. For comparison, the **K41** $-5/3$ power-law is also shown (solid-line). For clarity, the ordinate axes are at different scales in panel (b).

two methods to estimate α for the entire u and fBm records (sample sizes of 32,768) to produce local scaling frequency distributions shown in Figure 6 (a). Notice that the local scaling exponent distributions by the two methods are remarkably similar suggesting some robustness to the method of α estimation. This insensitivity is not surprising given the locality and non-spreading of the “cone of influence” evidenced in Figure 5 (a, bottom panel). Also, the u and fBm local scaling distributions are, for all practical purposes, identical and approximately Gaussian. We also note that in Bacry *et al.*⁷ the local scaling exponent distributions (digitized by us from their Figure 9) is also Gaussian [see Figure 6 (b)]. We also repeated the same calculations in Figure 6 (a) but using the Marr wavelet⁷ and found no difference in the u and fBm local scaling exponent distributions. Hence, such similarity in u and fBm local scaling exponent distributions cannot be an artifact of the wavelet basis.

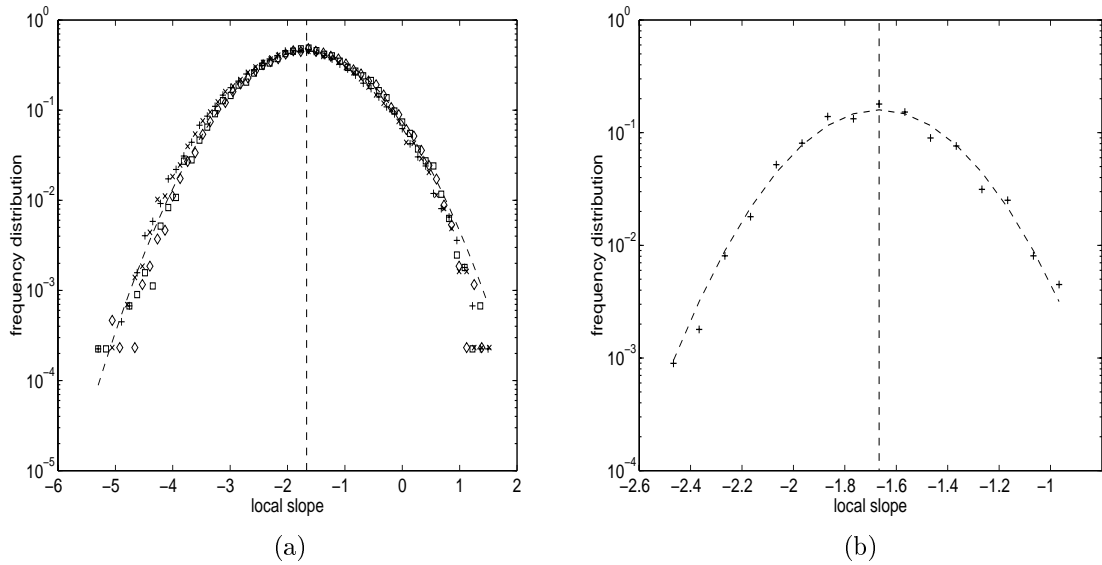


Figure 6: Panel (a): Frequency distribution of the local scaling exponents for fBm and u determined from regression and Bartlett’s method. The symbols are as follows: + and \times are for α ’s determined by regression and Bartlett’ method for u , diamonds and squares are α ’s determined by regression and Bartlett’s method for fBm . For comparison, a Gaussian distribution (dotted line) is also shown. The histograms are plotted on a logarithmic axis for clearer illustration of the histogram tails. The vertical dashed line is the $-5/3$ **K41** power-law. Panel (b): The histogram reported by Bacry *et al.*⁷ for the wind-tunnel experiment along with a Gaussian distribution (dotted line).

To further investigate whether such similarity in local scaling exponents for u and fBm is due to the method of α determination, we considered an alternative method,

known as the *method of ridges*^{6,38}. In this method, the local wavelet energy spectrum for u and fBm are computed and α s are derived by following local minima/maxima of the CWT energy (hereafter referred to as ridges). Along these ridges local slopes can be determined from the energy spectra E_r displayed in Figure 7 (a-b). The local scaling exponents determined from the ridges were not significantly different (not shown) for the fBm and u further supporting the analysis in Figure 6.

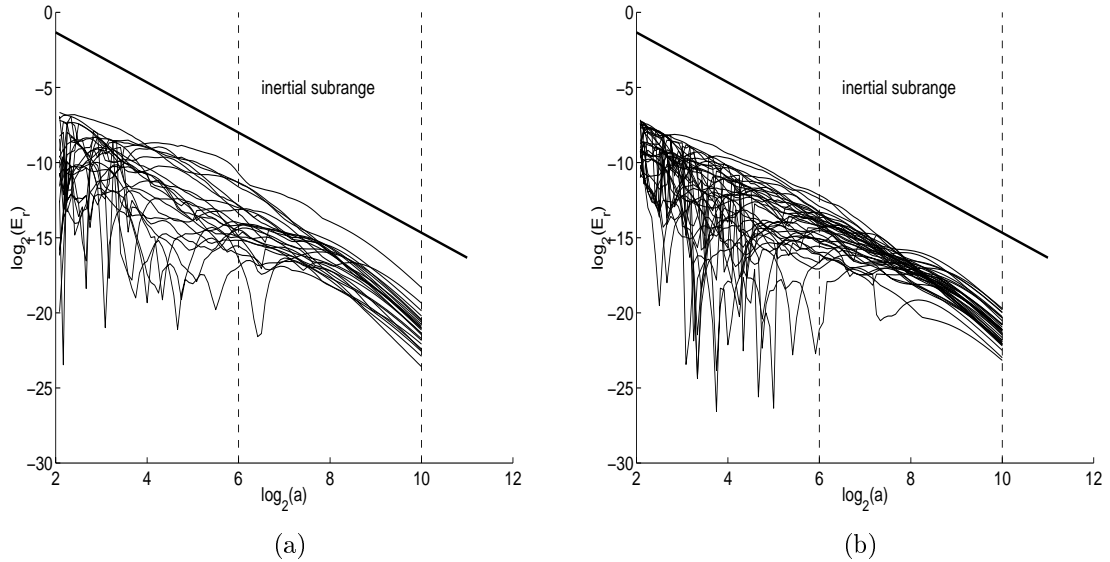


Figure 7: (a) Local energy spectra along ridges (E_r) as a function of frequency a for the u time series. (b) Same as (a) but for fBm time series.

In short, CWT was unable to discern fundamental differences in the univariate probability density functions of local scaling exponents derived from u and fBm time series.

5 Conclusion

This study demonstrated that both CWT and OWT do capture well intermittency effects and vortex stretching on global power-laws. In fact, the intermittency corrections to **K41** power-laws determined from OWT coefficients are in good agreement with the She-L ev eque vortex filament intermittency model. The latter model has no adjustable parameters.

Both wavelet transformation methods reproduced well the theoretical global power-laws for fBm . Hence, we see no advantage to utilizing CWT over the simpler OWT

for such applications. Furthermore, CWT was unable to discern any differences in local scaling exponent distributions derived from u and fBm time series.

Acknowledgment

This project was funded by the NSF DMS-9626159 award at Duke University. We thank D. Donoho for providing us with a beta version of WAVELAB 8.0 which was used in all the wavelet calculations. The MATLAB m-files and data sets are available upon request from the authors.

References

- ¹ K. R. Sreenivasan, R. A. Antonia, and D. Britz, *J. Fluid Mech.* **94**, 745 (1979).
- ² U. Frisch, *Turbulence* (Cambridge University Press, New York, 1995), p. 296.
- ³ M. Holschneider, *Wavelets: An Analysis Tool* (Oxford Science Publications, Oxford, 1995), p. 423.
- ⁴ *Wavelets and Applications*, No. 20 in *Research Notes in Applied Mathematics*, edited by Y. Meyer (Springer Verlag, New York, 1991).
- ⁵ Y. Meyer, *Wavelets and Operators, Cambridge Studies in Advanced Mathematics 37* (Cambridge University Press, New York, 1992).
- ⁶ S. G. Mallat, *A Wavelet Tour of Signal Processing* (Academic Press, San Diego, 1998).
- ⁷ E. Bacry *et al.*, in *Turbulence and Coherent Structures*, edited by O. Metais and M. Lesieur (Kluwer Academic Publishers, Norwell, MA, 1991), p. 450.
- ⁸ A. N. Kolmogorov, *Dokl. Akad. Nauk. SSSR* **4**, 299 (1941).
- ⁹ G. Parisi and U. Frisch, in *Turbulence and Predictability in Geophysical Fluid Dynamics*, edited by M. Ghil, R. Benzi, and G. Parisi (North-Holland, Amsterdam, 1985).
- ¹⁰ F. Argoul *et al.*, *Nature* **338**, 51 (1989).
- ¹¹ R. Everson, L. Sirovich, and K. Sreenivasan, *Phys. Let. A* **145**, 314 (1990).
- ¹² Z.-S. She, *Prog. Theor. Phys.* **130**, 87 (1998).
- ¹³ K. R. Sreenivasan and B. Dhruva, *Prog. Theor. Phys.* **130**, 103 (1998).
- ¹⁴ K. R. Sreenivasan and R. A. Antonia, *Annu. Rev. Fluid Mech.* **29**, 435 (1997).
- ¹⁵ M. Yamada and K. Ohkitani, *Prog. Theor. Phys.: Progress Letters* **86**, 819 (1990).
- ¹⁶ M. Yamada and K. Ohkitani, *Fluid Dynam. Res.* **8**, 101 (1991).
- ¹⁷ M. Yamada and K. Ohkitani, *Prog. Theor. Phys.* **86**, 799 (1991).
- ¹⁸ G. G. Katul, J. D. Albertson, C. C. Chu, and M. B. Parlange, in *Wavelets in Geophysics*, edited by ed. E. Foufoula (Academic Press, San Diego, 1994), pp. 9999–9999.
- ¹⁹ A. Benassi, in *Wavelets and Statistics, Lecture Notes in Statistics, 103*, edited by A. Antoniadis and G. Oppenheim (Springer Verlag, New York, 1995).
- ²⁰ P. Flandrin, *IEEE Trans. Inform. Theory* **35**, 197 (1989).
- ²¹ P. Flandrin, in *Wavelets and Their Applications*, edited by J. S. Byrnes, J. L. Byrnes, K. A. Hargreaves, and K. Berry (NATO ASI Series vol. 442, Kluwer, Dodrecht, 1992), pp. 121 – 142.
- ²² P. Flandrin, *IEEE Trans. Inform. Theory* **38**, 910 (1992).
- ²³ G. G. Katul and B. Vidakovic, *J. Atmos. Sci.* **55**, 377 (1998).
- ²⁴ M. Farge, *Annu. Rev. Fluid Mech.* **24**, 395 (1992).
- ²⁵ G. G. Katul *et al.*, *J. Geophys. Res.* **102**, 13409 (1997).
- ²⁶ G. G. Katul and J. Albertson, in *Bayesian Inference in Wavelet Based Models, Lecture Notes in Statistics*, edited by P. Müller and B. Vidakovic (Springer Verlag, New York, 1999), pp. 361–380.
- ²⁷ G. I. Taylor, *Proc. Roy. Soc. A* **CLXIV**, 476 (1938).

- ²⁸ F. Anselmet, Y. Gagne, E. J. Hopfinger, and R. A. Antonia, *J. Fluid Mech.* **140**, 63 (1984).
- ²⁹ J. D. Albertson, M. B. Parlange, G. Kiely, and W. E. Eichinger, *J. Geophys. Res.* **102**, 423 (1997).
- ³⁰ G. Katul, C. Hsieh, and J. Sigmon, *Bound. Layer Meteorol.* **82**, 49 (1997).
- ³¹ J. D. Albertson *et al.*, *Physics of Fluids* **10**, 1725 (1998).
- ³² A. N. Kolmogorov, *J. Fluid Mech.* **13**, 82 (1962).
- ³³ C. Meneveau, K. R. Sreenivasan, P. Kailasnath, and M.-S. Fan, *Phys. Rev. A* **41**, 894 (1990).
- ³⁴ C. W. V. Atta and W. Y. Chen, *J. Fluid Mech.* **44**, 145 (1970).
- ³⁵ Z. She and E. Leveque, *Phys. Rev. Lett.* **72**, 336 (1994).
- ³⁶ J. Liandrat and F. Moret-Bailly, *European Journal of Mechanics, B/Fluids* **9**, 1 (1990).
- ³⁷ J. Emerson and D. Hoaglin, in *Understanding Robust and Exploratory Data Analysis*, edited by D. Hoaglin, F. Mosteller, and J. Tukey (Wiley Interscience, New York, 1983).
- ³⁸ R. Carmona, W.-L. Hwang, and B. Torr sani, *IEEE Trans. Signal Process.* **45**, 2568 (1997).
- ³⁹ M. Farge *et al.*, *Fluid Dynam. Res.* **10**, 229 (1992).

Appendix: An Overview of Continuous and Discrete Wavelet Transformations

In this appendix, definitions and important properties of continuous wavelet transformations \mathcal{CWT} and their critically sampled counterparts are presented.

Let $\psi_{a,b}(x)$, $a \in \mathbb{R}^+$, $b \in \mathbb{R}$ be a family of functions defined as translations and re-scales of a single, square-integrable function $\psi(x)$,

$$\psi_{a,b}(x) = \frac{1}{\sqrt{|a|}} \psi\left(\frac{x-b}{a}\right). \quad (4)$$

The function ψ (called *the wavelet function*) is required to satisfy the *admissibility condition*,

$$C_\psi = \int_0^\infty \frac{|\Psi(\omega)|^2}{\omega} d\omega < \infty, \quad (5)$$

where $\Psi(\omega)$ is the Fourier transformation of $\psi(x)$.

Wavelet functions are usually normalized to have unit energy, i.e., $\|\psi_{a,b}(x)\| = 1$.

For any square-integrable (i.e. finite energy) function $f(x)$, the continuous wavelet transformation is defined as a function of two variables

$$\mathcal{CWT}_f(a, b) = \langle f, \psi_{a,b} \rangle = \int f(x) \overline{\psi_{a,b}(x)} dx.$$

Here the dilation and translation parameters, a and b , respectively, vary continuously over $\mathbb{R}^+ \times \mathbb{R}$.

When the admissibility condition is satisfied, i.e., $C_\psi < \infty$, it is possible to find the inverse continuous transformation via the relation known as *resolution of identity* or *Calderón's reproducing identity*,

$$f(x) = \frac{1}{C_\psi} \int_{-\infty}^{\infty} \int_0^{\infty} \mathcal{CWT}_f(a, b) \psi_{a,b}(x) \frac{1}{a^2} da db.$$

The continuous wavelet transformation is “energy conserving”,

$$\int_{-\infty}^{\infty} |f(x)|^2 dx = \frac{1}{C_\psi} \int_0^{\infty} \int_{-\infty}^{\infty} |\mathcal{CWT}_f(a, b)|^2 \frac{1}{a^2} db da.$$

The continuous wavelet transformation of a univariate function is a function of two variables. Clearly, such a transformation is redundant. To “minimize” the redundancy in the transformation, one can select discrete values of a and b to produce an invertible transformation. However, sampling that preserves all information about the decomposed function cannot be coarser than the *critical sampling*.

The critical sampling defined by

$$a = 2^{-j}, b = k2^{-j}, j, k \in \mathbb{Z}, \quad (6)$$

will produce a minimal basis. Any coarser sampling will not give a unique inverse transformation, that is, the original function will not be uniquely recoverable. For appropriate conditions applied to the wavelet function ψ , such sampling produces an orthonormal basis $\{\psi_{jk}(x) = 2^{j/2} \psi(2^j x - k), j, k \in \mathbb{Z}\}$. The coefficients of a function in the orthonormal wavelet basis represent orthonormal wavelet transformation, *OWT*.

One such basis function, used in this study, is generated by shifts and scales of a function

$$\psi(x) = \mathbf{1}(0 \leq x \leq 1/2) - \mathbf{1}(1/2 \leq x \leq 1).$$

This function is known as the Haar wavelet and is used frequently in turbulence research²³. Wavelet packets have also been proposed as an alternative source of basis functions in turbulence research³⁹. When compared with Haar's wavelet in the context of energy packing; only minor improvements were reported²³. Hence, for the purposes of this study only Haar's *OWT* is considered.